Geometrically accurate positive contrast of field disturbances using RAdial Sampling with Off-resonance Reconstruction (RASOR).

H. de Leeuw[1], P. R. Seevinck[1], C. Bos[2], G. H. van de Maat[1], and C. J. Bakker[1]
[1]Image Sciences Institute, Utrecht, Utrecht, Netherlands, [2]Philips healthcare

Introduction: With the advent of short-TE acquisitions, such as UTE and SWIFT, center-out radial acquisition schemes to fill k-space are gaining interest [1, 2]. Although these acquisitions minimize signal dephasing, they still suffer from field inhomogeneities through geometric distortion. Unlike for Cartesian encoding, geometric distortion for center-out radial acquisitions is directed radial and results in signal loss and blurring. In previous work [3] we showed that accurate depiction and localization of local field disturbers can be achieved by 3D center-out radial acquisition with off-resonance excitation and reception (RASOR). The off-resonance, however, depends on the object involved and needs proper tuning before imaging. In this work we present a refinement of RASOR in terms of efficiency and flexibility, by off-resonance reconstruction of on-resonance acquired images.

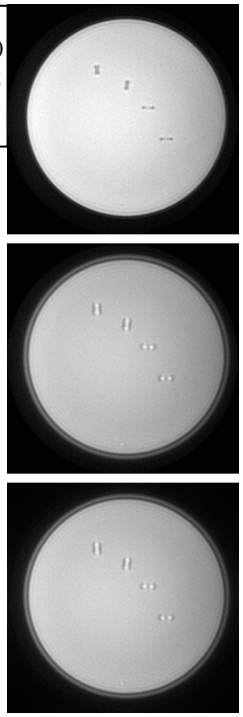

Figure 1: UTE image (top), acquired RASOR image (middle) and RASOR via post-processing (bottom) of phantom A. Field offsets were chosen at 300Hz.

Theory: In a three dimensional MRI experiment the signal (S) is given by:

$$S(k) = S(t) = \sum_{\vec{r}} \rho_0 e^{-i\gamma(\vec{G}\cdot\vec{r}+\Delta B(\vec{r}))t'} e^{-i\gamma\Delta B(\vec{r})TE} = \sum_{\vec{r}} \rho_0 e^{-i\gamma(\vec{G}\cdot\vec{r}+\Delta B(\vec{r}))t'} e^{-i\varphi(\vec{r})} \quad [1]$$

with ρ_0 the effective spin density, t' the time of acquisition (t'=t-TE), γ the gyromagnetic ratio, G the read-out gradient strength, **r** the position vector. The local field disturbance $\Delta B(\mathbf{r})$ is associated with phase $\varphi(\mathbf{r})$. In center-out radial acquisition schemes the gradient (G) is cycled to adopt each direction. As a consequence, local field distortions result in a radial displacement and hence smear of the signal. This radial displacement can be compensated for by introducing a frequency offset (δf), at the cost of radial smear of signal at locations without field inhomogeneity:

$$S(t) = \sum_{\vec{r}} \rho_0 e^{-i\gamma\vec{G}\cdot\vec{r}t'} e^{-i(\gamma\Delta B(\vec{r})+2\pi\delta f_0)t'} e^{-i(\gamma\Delta B(\vec{r})+2\pi\delta f_0)TE} = e^{-2\pi i\delta f_0 t'} \sum_{\vec{r}} \rho_0 e^{-i\gamma\vec{G}\cdot\vec{r}t'} e^{-i\gamma\Delta B(\vec{r})t'} e^{-i(\varphi(\vec{r})+\varphi_{\delta f_0})} \quad [2]$$

Equation 2 shows that the acquired data and the introduced off-resonance effects can be separated and that a frequency offset allows discrimination of dephasing effects and geometric distortion. Since encoding the off-resonance corresponds to the addition of a constant phase difference between locations in k-space, it can be taken out of the summation and thus accomplished via post processing. The compensation, as described by equation 2, only works at locations **r** at which $\gamma\Delta B(\mathbf{r}) = -2\pi\delta f_0$. At other locations the radial displacement will still occur, although either less or more than originally the case. The radius of displacement is given by $|\gamma\Delta B+2\pi\delta f_0|/|G|$. Due to the center-out radial acquisition, the signs do not matter. The larger the radius of displacement, the smaller the intensity from one point-source, since the intensity of a single point is spread over the area of a sphere with as radius the radius of displacement. While in realistic cases the field cannot be described by a single off-resonance, each field disturbance will give a displacement with a width larger than its size. This point-spread obviously varies in amplitude and width, and will be smallest for $2\pi\delta f_0$ approximately equal to the $-\gamma\Delta B$ at the edge of the field perturber. Further off-resonance an intensity hotspot can occur at the center of the positive or negative fields, where the point spread function of multiple field deviations overlap.

Materials & Methods: Two phantoms were used to show the equivalence of the hardware and software variant of RASOR and demonstrate their characteristics. The phantoms consisted of cylindrical gel phantoms with a diameter and height of 10cm, filled with Agar gel (2%) doped with 32mg/l $MnCl_2.4H_2O$. In phantom A, 4 brachytherapy seeds (0.8×4.5mm), used for radiotherapy treatment planning [4], were placed. Two of the seeds were placed approximately parallel and two approximately perpendicular to the main magnetic field. In phantom B randomly four glass spheres (diameters 14mm (2x), 13mm and 8mm) were dispersed. Both phantoms were placed with the principal axis perpendicular to the main magnetic field. Imaging was done on a 1.5T clinical whole body MR system (Achieva 1.5T, Philips Healthcare, Best, The Netherlands). The data was collected with a multi-echo (3 echoes) 3D radial UTE pulse sequence. Scan parameters included FOV 128x128x128 mm^3, scan matrix 128x128x256, reconstruction matrix 256^3, radial sampling 100%, TR 25ms, TE_1 0.20ms and ΔTE 3.9 ms, flip angle 10°, NSA 1 and read-out bandwidth 300 Hz/pixel, resulting in a scan duration of 7 minutes and 8 seconds per scan. Multiple off-resonance images of both phantoms were acquired. Post-processing RASOR was implemented by adding the phase (s.f. equation 2), to the regridded k-space. Post-processing was performed on a Dell optiplex 760 with an Intel Q8300 quadcore processor (2.5GHz), with 8 GB RAM and took less than a minute for a dataset of 256×256×256. Multiple off-resonances were post-processed in the range of -1000 to +2100 Hz.

Results & Discussion: Figure 1 shows phantom A, acquired without and with a frequency offset. From top to bottom, the figure shows the original -on resonance- image, the image acquired 300Hz off-resonance, and the calculated image 300Hz off-resonance. As expected from equation 2, acquisition and post processing RASOR show excellent agreement. Similar results were obtained for phantom B (not shown). Small discrepancies between measurements and calculations were observed and can be ascribed to the absence of the phase offset and the usage of the regridded, instead of the original k-space data for post processing RASOR. The RASOR images in figure 1 visualize the seeds with high positive contrast. The dots for the rods perpendicular to B_0 are approximately 4mm apart, in close correspondence with the size of the seeds. The length of the line for seeds parallel with B_0 overestimates the size of the seeds, due to an off-resonance. A more detailed illustration of the sensitivity of the point spread function is given in figure 2.

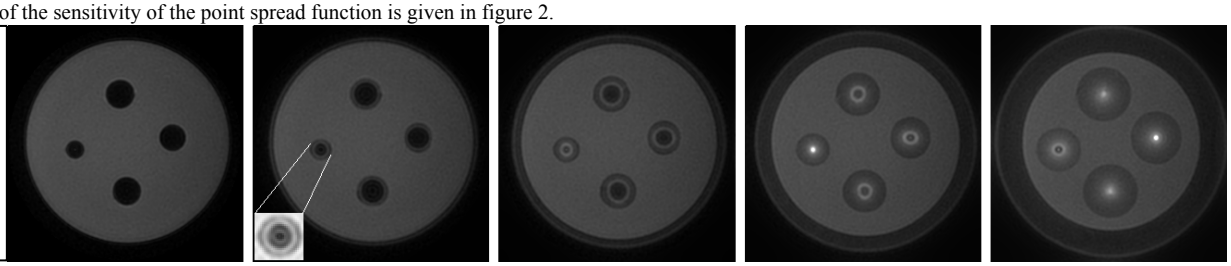

Figure 2: Software RASOR images of phantom B reconstructed with offset frequency, from left to right, 0, 210, 600, 1200 and 2100 Hz.

In figure 2 from left to right an offset frequency of 0, 210, 600, 1200 and 2100 Hz is applied to images by post processing RASOR. In the zero offset image -the original UTE image- the point spread function around the spheres is wide and therefore the white ring around the spheres is not clearly visible. That the introduced field offset introduces a radial displacement of the, normally on-resonance, background is clearly visible in the ring around the container, which increases in size with increasing off-resonance. At the same rate, the gel in the container appears to become smaller, also due to the radial displacement. Also note the lower intensity of the displaced signal. For the left sphere in figure 2 the point-spread is clearly increasing from left to right, i.e. the high signal ring is becoming broader. At an off-resonance of 210Hz, the point spread is smallest, resulting in a peak-to-peak distance (brightest white ring in insert fig 2) of approximately 8.0 mm. Figure 2 shows that, at one particular off-resonance, the point-spread ring is focused into a single hyper-intensity. It is straightforward to show that this single point-intensity is always located at the centre of the fields, in this case also the center of the studied object. For the larger spheres a similar description applies, although the sphere radius and therefore the frequency of centering differ.

In summary we have shown that by studying the point spread of the local field deviation, both the size and location of a local field disturber can be extracted. Since RASOR can be obtained through post-processing, the information on the field can be projected onto the original image without the need for registration or additional acquisition time. Up to an off-resonance related phase factor, the post-processing implementation of RASOR yields the same results as RASOR by acquisition. To increase the specificity of RASOR further, the background might be suppressed by using long T_2 suppression techniques. Although in this abstract only results are shown for UTE sequences, post-processing RASOR is generally applicable to center-out radial acquisitions. We therefore expect that this post processing implementation of RASOR is a valuable modification to the acquisition RASOR and may find utility in applications that need accurate depiction and localization of local field disturbances.

Conclusion: Geometrically accurate depiction and localization of local field disturbers can be achieved by a 3D center-out radial acquisition with off-resonance acquisition or reconstruction. The advantage of the reconstruction is a more precise determination of the shape and location, while retaining the original image.

References: [1] D. Idiyatullin et al. J*MRI* 2006;181:342-349 [2]M.D. Robson et al. *J Computer Assisted Tomogr* 2003;27:825-846 [3] P.R. Seevinck *Dissertation thesis ISBN: 978-90-393-5223-6;* Gildeprint drukkerijen, Enschede 2009 [4] M.E. Miquel et al. *Phys. Med. Biol* 2006; 51(5):1129-1137